RMetS
Royal Meteorological Society

Using enstrophy advection as a diagnostic to identify blocking-regime transition

A. D. Jensen* and A. R. Lupo

Department of Soil, Environmental, and Atmospheric Sciences, University of Missouri–Columbia, MO, USA

*Correspondence to: A. D. Jensen, Department of Soil, Environmental, and Atmospheric Sciences, 302 Anheuser Busch Natural Resources Building, University of Missouri, Columbia, MO 65211, USA. E-mail: jensenad@missouri.edu

This article proposes a method to identify blocking onset and decay by means of two stability indicators: enstrophy advection and its integral. The key to this technique is the use of local Lyapunov exponents for the barotropic vorticity equation, which can be approximated by the integral of enstrophy (IRE) over a fixed, finite region. The IRE can then be viewed as a measure of stability. However, by differentiating the IRE with respect to time, two measures of stability can be derived to assess blocking onset and decay: (i) the integral of enstrophy advection (DIRE), for which a time series is used to assess stability, and (ii) enstrophy advection, for which contours are plotted in conjunction with 500 hPa heights to locate blocking. One year's worth of Northern Hemisphere blocking events from July 2011–July 2012 are studied to demonstrate that the integral of enstrophy advection is a useful diagnostic. In particular, time series of IRE and DIRE for four of the blocking cases are presented, while contour plots of enstrophy advection for one case are presented. In all cases studied, the diagnostics were seen to detect the instability in an incipient blocking event and in its decay.

Key Words: blocking; regime transition; enstrophy; block onset

Received 27 February 2013; Revised 19 June 2013; Accepted 18 July 2013; Published online in Wiley Online Library

1. Introduction

The phenomenon of blocking can be described as a quasi-stationary atmospheric state with a quasi-barotropic structure (see Dymnikov *et al.*, 1992). Notwithstanding the nearly stationary nature of blocking events, it has been shown that, because of the unstable nature of the flow during block onset and decay, forecasts for regions in and near the block are often less accurate, (e.g. Tibaldi and Molteni, 1990; Pavan *et al.*, 2000; Watson and Colucci, 2002; Frederiksen *et al.*, 2004). However, recent results suggest that, with the use of certain global stability criteria, both the onset and decay of blocking may be identified with certainty (see e.g. Lupo *et al.*, 2007, 2012; Athar and Lupo, 2010). Now, Dymnikov *et al.* (1992) showed that in a quasi-barotropic flow the sum of the positive local Lyapunov exponents can be approximated by integrating enstrophy (squared vorticity) over a finite bounded region. This quantity has been termed area-integrated enstrophy (IRE) and has been used to determine the stability or predictability within a planetary flow regime (Lupo *et al.*, 2007, 2012; Athar and Lupo, 2010).

One potential disadvantage of this technique is that it is not apparent when the enstrophy will be increasing or decreasing. In contrast, with the derivative of the IRE (DIRE), the change in instability can be identified by the sign: local extrema can be found on a time series crossing the time axis. In addition, contours of enstrophy advection may be used to locate blocking. In this work we have identified the enstrophy advection and its integral as useful diagnostics in identifying blocking-regime transition.

The purpose of this work is the following: (i) to develop techniques that extend the results of Lupo *et al.* (2007) and demonstrate that these techniques (enstrophy advection and DIRE) can be used to detect blocking onset and decay; and (ii) to demonstrate the ways in which contours of enstrophy advection behave during blocking onset and decay, throughout the duration of the event, and that they may be useful in detecting blocking events. Throughout this study we compare the results obtained by means of enstrophy advection and its integral with the previous techniques used and developed in Lupo *et al.* (2007, 2012) and Athar and Lupo (2010).

The outline of the article is as follows. In section 2 we present the stability indices to be used in this study: the use of enstrophy advection and its integral to identify an increase or decrease in instability is also presented. In section 3 we present the dataset used in the study and the criteria used to determine whether a flow is in a blocked state. In section 4 we present our results for the integral of enstrophy advection (DIRE) and provide contours of enstrophy advection. We discuss our findings and summarize our conclusions in section 5.

2. Diagnostic

2.1. Local Lyapunov exponents

To explain the use of IRE, DIRE and enstrophy advection as indicators to assess flow instability, the local Lyapunov exponents for the barotropic vorticity equation must first be considered. We

therefore offer a brief description of local Lyapunov exponents and describe an approximation of the local Lyapunov exponents of the barotropic vorticity equation. In general, local Lyapunov exponents are defined by $\lambda_i(\zeta_0, T) = [1/(2n)] \log \nu_i$ for an initial vorticity field ζ_0 and time $T = n\Delta t$. The ν_i are the eigenvalues of M^*M, where $M = \prod_{k=-n}^{k=n} A(k\Delta t)$ and $A(t)$ is the linearization operator of the barotropic vorticity equation at $\zeta(t)$. The local Lyapunov exponents thus provide a measure of the rate of divergence or separation of nearby trajectories for small times.

We now sketch the argument given in Dymnikov *et al.* (1992), that the IRE is approximated by the sum of the positive local Lyapunov exponents of the barotropic vorticity equation for an incompressible, frictionless flow. Since incompressibility is assumed, a streamfunction Ψ may be found, where $\Delta\Psi = \zeta$, and Δ is the Laplacian operator. The barotropic vorticity equation can then be written in the form

$$\frac{\partial \Delta\Psi}{\partial t} + J(\Psi, \Delta\Psi) = 0.$$

To model blocked flow, a streamfunction is considered, of the form

$$\Psi = \overline{\psi}(y) + \psi'(x, y),$$

where

$$\psi'(x, y) = \psi(y)\mathrm{e}^{\mathrm{i}kx}.$$

Thus, Ψ describes a zonal flow with superimposed stationary waves.

It was found in Dymnikov *et al.* (1992) that, by using the streamfunction, the operator $S = A + A^*$, where A is the linearization operator for the barotropic vorticity equation, can be written as $S = -\mathrm{i}kK$, where K is a skew-symmetric operator. Thus, the eigenvalues of the operator K^2 are studied, where the eigenvalues of K^2 are equal to the square of the eigenvalues of S. A Crank–Nicholson scheme (see Durran (2010) for an explanation of this scheme) can be applied to the linearized barotropic vorticity equation to obtain the result that the sum of the positive local Lyapunov exponents is determined by the integral of enstrophy (IRE), where the integral is over a finite and bounded region (in Dymnikov *et al.* (1992) it was the whole Northern Hemisphere). It was also shown that the approximation should hold for small times only.

2.2. Previous techniques: IRE

Recent work (Dymnikov *et al.*, 1992; Lupo *et al.*, 2007, 2012; Athar and Lupo, 2010) based on the idea that changes in the planetary-scale flow can lead to blocking-regime transition (Hansen and Sutera, 1993; Haines and Holland, 1998) has shown the value of the IRE as a diagnostic for block onset and block decay. In Lupo *et al.* (2007), three winter season blocking events in the Southern Hemisphere were considered. For these events, the IRE was observed to increase sharply at block onset, indicating an increase in planetary flow instability. The IRE was then observed to decrease to a local minimum. Finally, the IRE was seen to increase again at block decay. Moreover, in Athar and Lupo (2010) the IRE was used to examine a three-year period (126 events) of blocking occurrences across the entire NH with similar results. It was found in every case, that there was a relative maximum in the IRE field at block onset and decay. Also, while studying the relative influence of planetary- and synoptic-scale interactions in blocking (see Shutts, 1983), Athar and Lupo (2010) also compared Northern Hemisphere values of the IRE with blocking-region values in a $40^\circ \times 60^\circ$ box. In this study, we calculate only Northern Hemisphere values of the IRE (as in Dymnikov *et al.*, 1992), since our purpose is to extend the previous techniques rather than study the relative influence of the planetary and synoptic scales. In Lupo *et al.* (2012), the blocking events that occurred over the European part of Russia were considered. The dynamical behaviour of these events yielded similar results.

2.3. Enstrophy advection and its integral

Now we show how enstrophy advection and its integral can be used to assess stability changes. As was shown in Dymnikov *et al.* (1992) and as sketched above, we may take

$$\sum_{\lambda_i > 0} \lambda_i \approx \int \zeta^2 \tag{1}$$

as a useful approximation, where the integral is taken over the entire Northern Hemisphere. Since the λ_i change with time, we may consider the change of their sum, $\sum_{\lambda_i>0} \lambda_i$, with time (see Shadden *et al.* (2005) for a proof that finite-time Lyapunov exponents are C^1 in time). We differentiate Eq. (1) under the integral to obtain

$$\frac{\partial \left(\sum_{\lambda_i>0} \lambda_i\right)}{\partial t} \approx \frac{\partial}{\partial t} \int \zeta^2 = -\int \mathbf{V} \cdot \nabla \zeta^2, \tag{2}$$

where we have assumed an incompressible frictionless barotropic flow. Therefore, the change in the stability characteristic over time can be approximated by $-\int \mathbf{V} \cdot \nabla \zeta^2$. The interpretation is straightforward. If the integral is negative, instability is decreasing. If the integral is positive, instability is increasing. Regions in which $-\int \mathbf{V} \cdot \nabla \zeta^2$ changes from positive to negative over time are where a local maximum in instability is expected. In this study we calculate the DIRE over the Northern Hemisphere in order to compare the results with the IRE.

Moreover, since the quantity $-\mathbf{V} \cdot \nabla \zeta^2$ determines the sign of the integral, we may also consider the enstrophy advection, $-\mathbf{V} \cdot \nabla \zeta^2$, as an indicator of increasing or decreasing instability. The interpretation is analogous to that of the integral of enstrophy advection. If $-\mathbf{V} \cdot \nabla \zeta^2 < 0$, the flow instability is decreasing. On the other hand, if $-\mathbf{V} \cdot \nabla \zeta^2 > 0$, the flow is becoming more unstable.

3. Data and methods

3.1. Dataset

The dataset used for the calculations of IRE, enstrophy advection and its integral was the NCEP–NCAR gridded reanalysis data (Kalnay *et al.*, 1996). The 0000 UTC NCEP–NCAR reanalyses of gridded ($2.5^\circ \times 2.5^\circ$) u and v components of the wind at 500 hPa were used in all calculations. The 0000 UTC 500 hPa geopotential heights were also used for the contour plots of enstrophy advection below. We note that all calculations were performed using spherical coordinates over the entire Northern Hemisphere, even though, for simplicity all equations appear in a Cartesian framework.

3.2. Blocking definition

The blocking criterion given in Lupo and Smith (1995) was used to detect the onset and decay times for the blocking events used in this study. In this criterion, blocking is defined to occur if the following conditions hold: (i) the Rex critiera (see Rex, 1950a,b) for blocking with minimum duration of the blocking event of 5 days is satisfied; (ii) a negative or small positive LO 83 index (see Lejenas and Okland, 1983) must be present on a Hovmöller diagram; (iii) conditions (i) and (ii) are satisfied from 24 h after onset to 24 h before termination; (iv) the blocking should be north of 35°N and the ridge should have an amplitude of greater than 5° latitude; (v) blocking onset is defined to occur when condition (iv) and either conditions (i) or (ii) are satisfied; and (vi) termination is designated at the time the event fails condition (v) for a 24 h period or longer.

4. Results

4.1. IRE and DIRE

The blocking definition given in Lupo and Smith (1995) was used to determine the blocking-regime transition times for the 31 Northern Hemisphere blocking events from July 2011–July 2012.

The behaviour of the 31 events studied was similar to others analyzed in previous work (e.g. Lupo *et al.*, 2007, 2012; Athar and Lupo, 2010). The relevant data are summarized in Table 1. Now, as cases representative of the others, the blocking events from January 2012 are presented (see Table 2, where the blocking intensity (BI) definition is given in Wiedenmann *et al.* (2002)). The Northern Hemisphere time evolution of IRE for the month of January 2012 is shown in Figure 1. As described in section 2, local maxima in the IRE field represent instability in the planetary-scale flow. There is a marked local maximum in IRE between 5 and 7 January at the time of block onset for the first blocking event listed in Table 2. There are other such local maxima for the other blocking events: 8–11 January, 11–13 January, 16–18 January. Moreover, the local maxima at the time of block decay for each event can also be seen.

Table 1. Number of blocking events from July 2011–July 2012 for which the integral of enstrophy advection (i) changed from positive to negative on the day of block onset as determined by the Lupo–Smith criterion, (ii) changed from positive to negative within ± 1 day or (iii) ± 2 days, or (iv) remained positive at onset (decay), indicating increasing instability.

	Exact	± 1 day	± 2 days	Remained positive
Onset	9	8	6	8
Decay	9	9	4	9

Table 2. January 2012 blocking events with block intensity and longitude at block onset.

Start date	End date	BI	LON
6 January	12 January	3.69	60 E
9 January	16 January	3.55	20 W
12 January	27 January	5.01	130 W
17 January	29 January	3.61	60 E

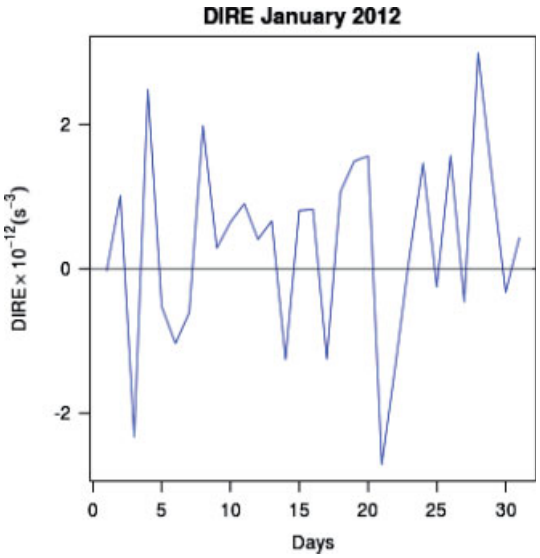

Figure 2. Time series of area averaged DIRE using Eq. (2) for the month of January 2012. Block onset for the events in Table 2 can be seen as positive values or positive values crossing the time axis to negative values and similarly for block decay. This figure is available in colour online at wileyonlinelibrary.com/journal/qj

The behaviour of the DIRE as the derivative of the IRE can be seen in the Northern Hemisphere time series of the integral of enstrophy advection (see Figure 2): where there is a local maximum or minimum in the IRE field, the DIRE field is at or near zero. Between 5 and 7 January, the IRE field attains a local maximum, while the DIRE field crosses zero from positive to negative values, indicating a local maximum in instability. We note that the DIRE does not cross the time axis from positive to negative values at block onset for the 9–17 January block but stays positive, indicating increasing instability. However, for the other two blocks in Table 2, the DIRE crosses the time axis near block onset. Similar behaviour can be seen at block decay for all of the blocking events listed in Tables 1 and 2 (See Figure 3 for the IRE and DIRE together).

4.2. Contours

As described in section 2.3, the enstrophy advection can also be used as an indicator of instability. The difference here is that,

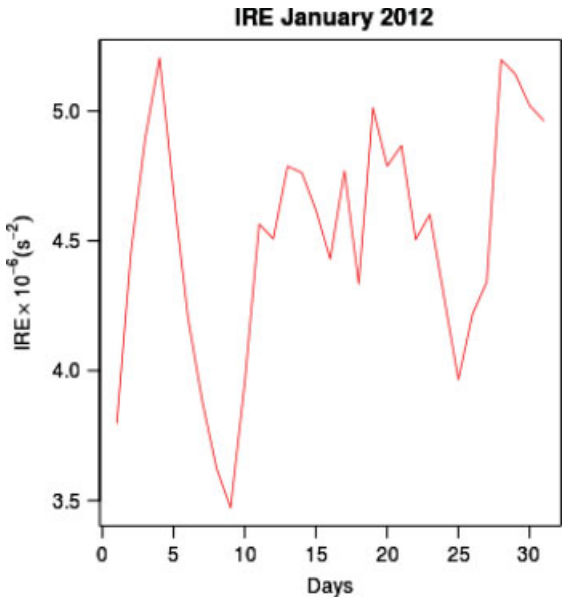

Figure 1. Time series of area-averaged IRE using Eq. (1) for the month of January 2012. Block onset for the events in Table 2 can be seen as local maxima and block decay can also be seen for the events as local maxima. This figure is available in colour online at wileyonlinelibrary.com/journal/qj

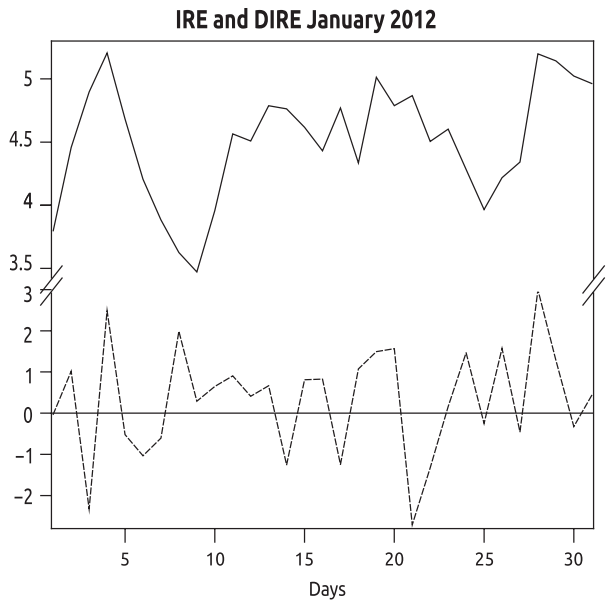

Figure 3. Time series of area-averaged IRE and DIRE for the month of January 2012. The solid line is the IRE from Figure 1 and the dashed is the DIRE from Figure 2.

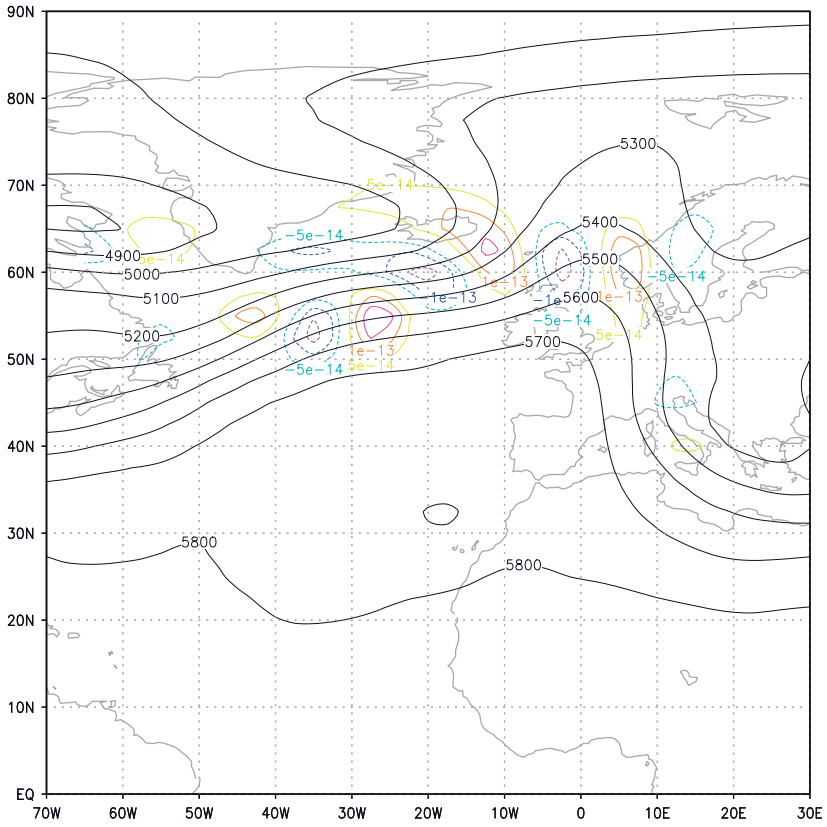

Figure 4. Contours of enstrophy advection for 9 January. Block onset instability is shown. Solid contours are positive enstrophy advection, dashed contours are negative enstrophy advection. The 500 hPa heights are shown in solid black. This figure is available in colour online at wileyonlinelibrary.com/journal/qj

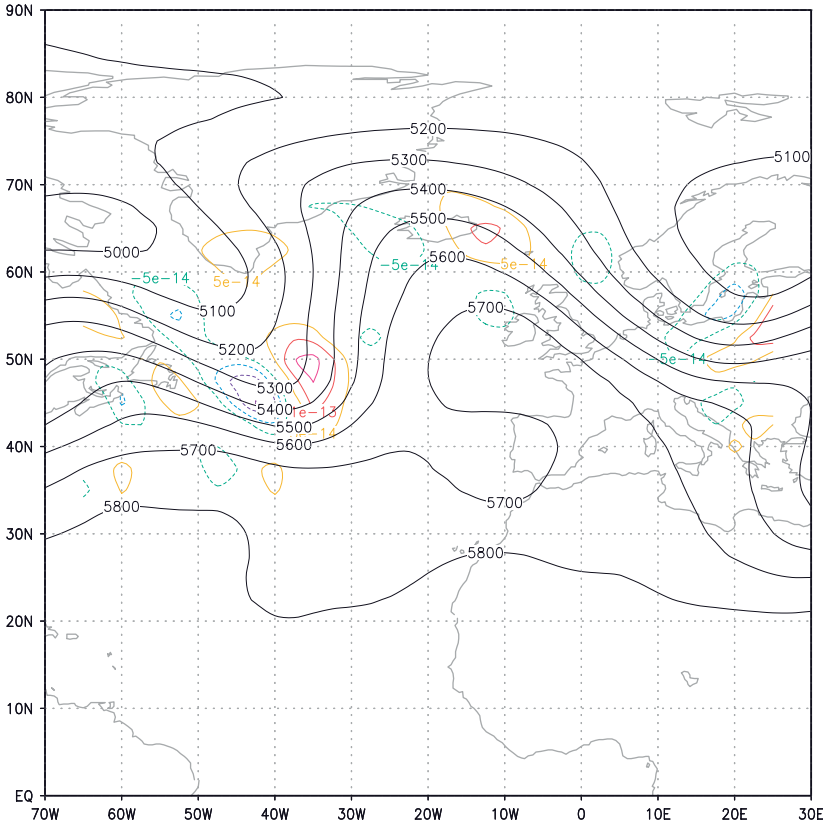

Figure 5. Contours of enstrophy advection for 13 January. By this time the block has reached a mature stage. The 500 hPa heights are shown in solid black. This figure is available in colour online at wileyonlinelibrary.com/journal/qj

instead of approximating the sum of the change of the local Lyapunov exponents by the integral of enstrophy advection, only the enstrophy advection is considered. Instead of a time series, it is convenient to plot contours of enstrophy advection to locate blocking regions. Thus, instead of a single number characterizing an entire hemisphere, the contours indicate where the instability in a region is located. As mentioned in section 3.1, all calculations were performed over the entire Northern Hemisphere. However, the latitude–longitude box in Figures 4–7 was chosen to highlight the blocking region as opposed to the whole hemisphere. In this work, only the contours of enstrophy advection for the block from 9–17 January 2012 are provided. (We note that the contours of

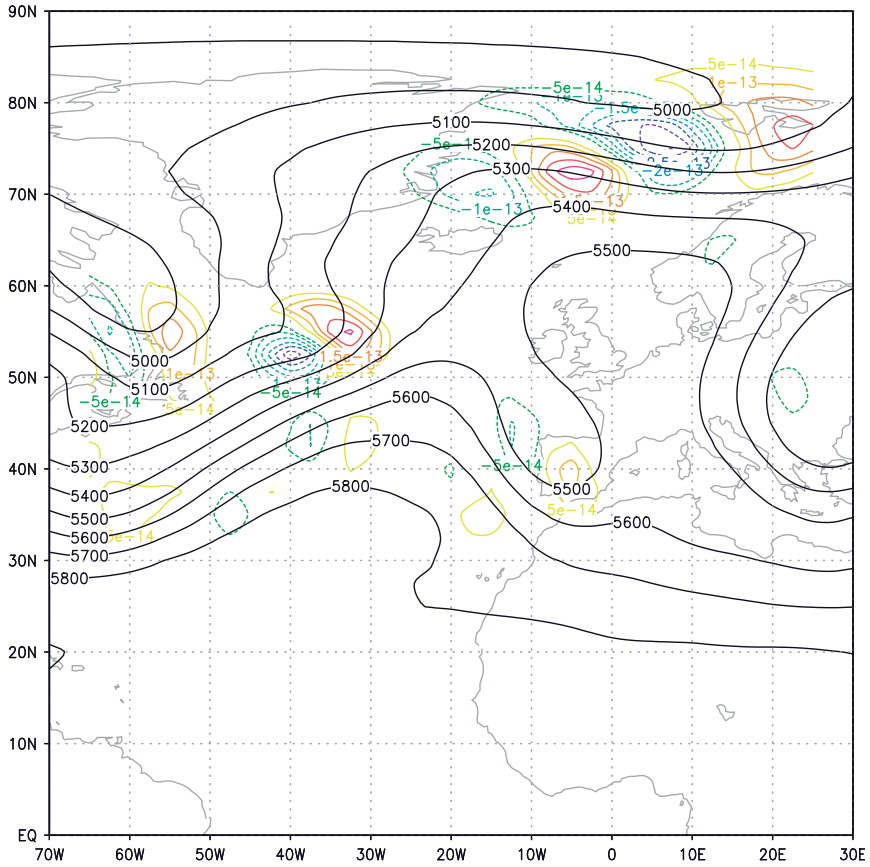

Figure 6. Contours of enstrophy advection for 16 January. Block decay instability is shown. The 500 hPa heights are shown in solid black. This figure is available in colour online at wileyonlinelibrary.com/journal/qj

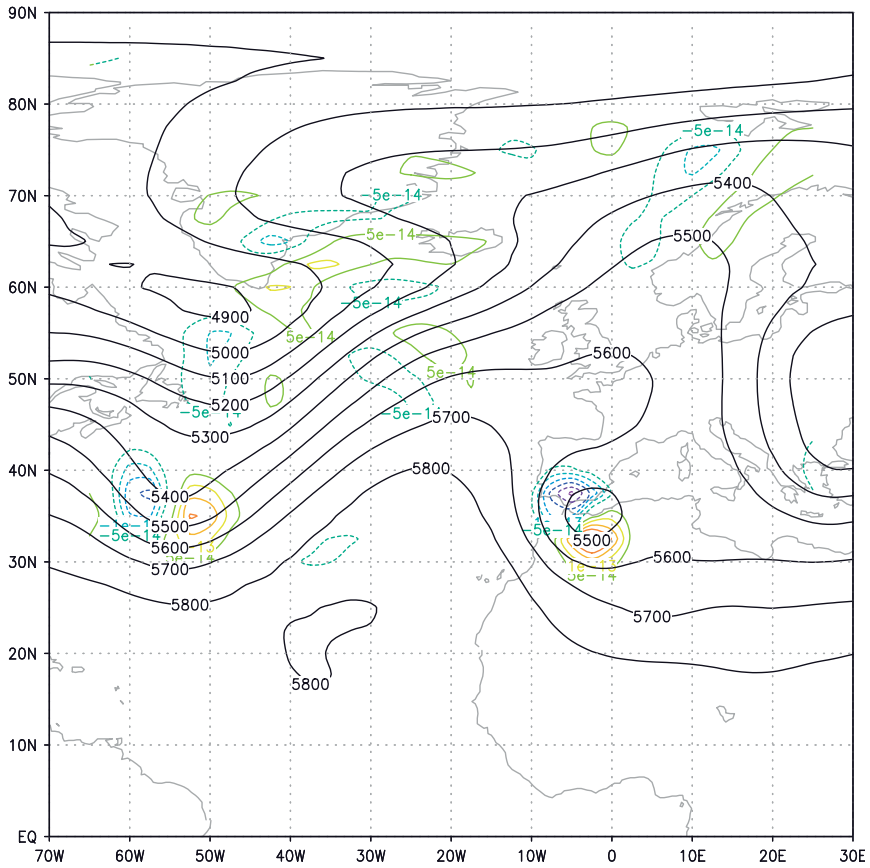

Figure 7. Contours of enstrophy advection for 17 January. Block decay instability is shown. The 500 hPa heights are shown in solid black. This figure is available in colour online at wileyonlinelibrary.com/journal/qj

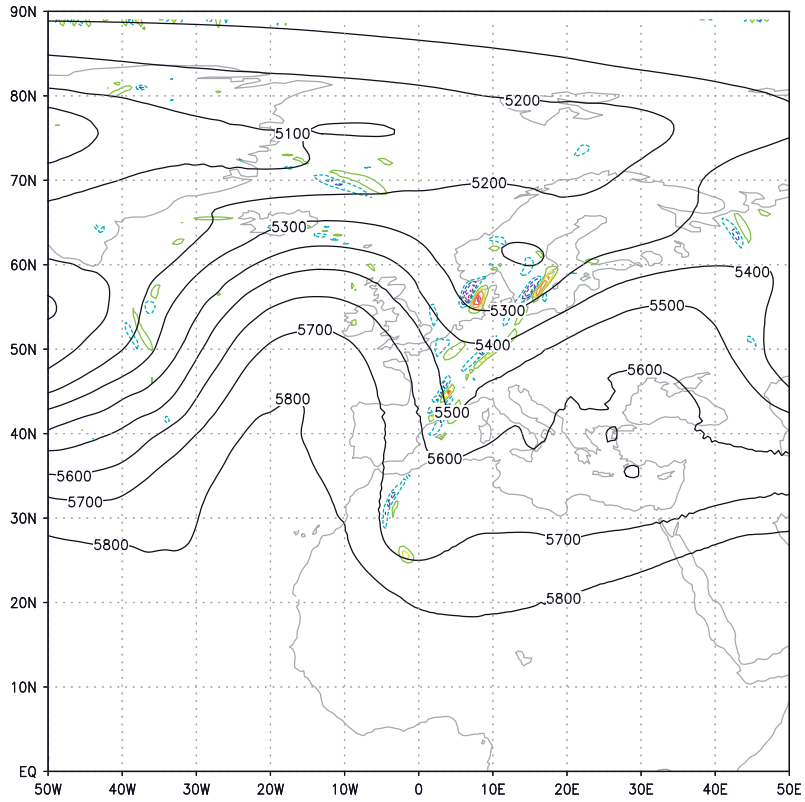

Figure 8. Contours of enstrophy advection for 2 January from the GFS model (0.5°). The 500 hPa heights are shown in solid black. This figure is available in colour online at wileyonlinelibrary.com/journal/qj

the other blocking events listed in Table 2 are analogous to the 9–17 January block.) The instability predicted by the IRE at block onset (Lupo *et al.*, 2007) can be seen (see Figure 4) as contours of enstrophy advection north of the blocking region. The increasing instability can be seen as solid contours of enstrophy advection, while decreasing instability can be seen as dashed contours. We note that all contours represent changing instability, however. By 13 January (see Figure 5), the blocking event has reached a mature stage. Contours of enstrophy advection can be seen north of the blocking region and along the sides of the ridge. Finally, in Figures 6 and 7, the instability at block decay as predicted in Lupo *et al.* (2007) and as indicated in Figures 1 and 2 can be seen. As the block decays, contours of enstrophy advection are located mainly to the north and west.

5. Discussion and conclusions

An extension of the methods developed in Lupo *et al.* (2007, 2012) and Athar and Lupo (2010) was used to assess the onset and decay of blocking. In the cases studied, the integral of enstrophy advection (DIRE) performed similarly to the IRE in detecting block onset and decay, although the interpretation is different since DIRE is the derivative of IRE. One advantage of the DIRE over the IRE is that the DIRE can assess the change in instability by means of its sign: extrema in the IRE field occur where the DIRE crosses the time axis. However, the DIRE may not be more effective when used alone. The IRE and the DIRE used together give a more accurate picture of stability. It is worth noting that a weakness in both of these techniques is that if the onset and decay of two or more blocks overlap then it may be difficult to assess the changing instability. It is also important to note that the techniques developed here do not establish the existence of blocking unambiguously. Some other criterion, such as the one described in Lupo and Smith (1995), is needed to establish the existence of a blocking event.

Now, contours of enstrophy advection appear to be a useful tool to identify blocking events. The contours of enstrophy advection hug the ridges associated with the blocking episode studied throughout the duration of the event. This may make visual block identification easier when contours of enstrophy advection are plotted with 500 hPa heights. Moreover, this technique does not suffer from the weakness (that of overlapping blocking onset and decay times) of the IRE and DIRE mentioned above, since the contours can be used to identify blocking in a region rather than assigning a number to indicate the stability of a whole hemisphere (IRE and DIRE). The enstrophy advection also may affect the nature of the blocking event in a physical sense (this will be explored in another article). In addition, the enstrophy advection does not appear to penetrate the centre of the blocking region, which may be due to physical processes to be explained in future research, in which we plan to study more cases of blocking-regime transition using the techniques developed here. These techniques may also be used in forecasting models. As an example, in Figure 8 contours of enstrophy advection for block onset can be seen for the blocking event from 2–8 January 2013, with data from the Global Forecast System (GFS) 0.5° model. We note that analysis of the behaviour in models of the techniques developed here is subtle and will be explored in further research. The enstrophy advection may have applications outside blocking, but because of the assumptions imposed, the applicability is restricted to mainly synoptic-scale phenomena.

The purpose of this work was to develop techniques (DIRE and enstrophy advection) by means of which blocking events and blocking-regime transition can be more successfully identified, which may lead to more accurate forecasting of blocking. The simplicity of enstrophy advection as a stability index may make it useful as a diagnostic in forecasting blocking-regime transition.

In Dymnikov *et al.* (1992), blocking was described as a quasi-stationary state with a quasi-barotropic structure. In this short work, a barotropic structure has been employed as a model of the atmosphere to derive measures of stability/instability to identify blocking onset and decay: the enstrophy advection and its integral. A time series of the values of the integral of enstrophy advection (DIRE) was used to identify blocking onset and decay for four Northern Hemisphere blocking events from January 2012. Plots of enstrophy advection were provided for the 9–17 January 2012 Northern Hemisphere blocking event. As can be seen in the plots,

the enstrophy advection locates the instability in a blocking event. The enstrophy advection and its integral (DIRE) were both found to be useful diagnostics in identifying blocking-regime transition.

Acknowledgements

The authors thank the editor and the two anonymous reviewers for their helpful comments and insight, which have improved the clarity and strength of this article.

References

Athar H, Lupo AR. 2010. Scale and stability analysis of blocking events from 2002–2004: A case study of an unusually persistent blocking event leading to a heat wave in the Gulf of Alaska during August 2004. *Adv. Meteorol.* **2010**: Article ID 610263; 15pp, Doi: 10.1155/2010/610263.

Durran DR. 2010. *Numerical Methods for Fluid Dynamics: With Applications to Geophysics*. Springer: New York, NY.

Dymnikov VP, Kazantsev YV, Kharin VV. 1992. Information entropy and local Lyapunov exponents of barotropic atmospheric circulation. *Izv. Atmos. Oceanic Phys.* **28**: 425–432.

Frederiksen JS, Collier MA, Watkins AB. 2004. Ensemble prediction of blocking regime transitions. *Tellus* **56A**(:): 495–500.

Haines K, Holland AJ. 1998. Vacillation cycles and blocking in a channel. *Q. J. R. Meteorol. Soc.* **124**: 873–897.

Hansen AR, Sutera A. 1993. A comparison between planetary-wave flow regimes and blocking. *Tellus* **45A**: 281–288.

Kalnay E, Kanamitsu M, Kistler R, Collins W, Deaven D, Gandin L, Iredell M, Saha S, White G, Woollen J, Zhu Y, Leetmaa A, Reynolds R, Chelliah M, Ebisuzaki W, Higgins W, Janowiak J, Mo KC, Ropelewski C, Wang J, Jenne R, Joseph D. 1996. The NCEP/NCAR 40-year reanalysis project. *Bull. Am. Meteorol. Soc.* **77**: 437–471.

Lejenas H, Okland H. 1983. Characteristics of Northern Hemisphere blocking as determined from a long time series of observational data. *Tellus* **35A**: 350–362.

Lupo AR, Smith PJ. 1995. Climatological features of blocking anticyclones in the Northern Hemisphere. *Tellus* **47A**(:): 439–456.

Lupo AR, Mokhov II, Dostoglou S, Kunz AR, Burkhardt JP. 2007. The impact of the planetary scale on the decay of blocking and the use of phase diagrams and enstrophy as a diagnostic. *Izv. Atmos. Oceanic Phys.* **42**: 45–51.

Lupo AR, Mokhov II, Akperov MG, Cherokulsky AV, Athar H. 2012. A dynamic analysis of the role of the planetary and synoptic scale in the summer of 2010 blocking episodes over the European part of Russia. *Adv. Meteorol.* **2012**: Article ID 584257; 11pp, Doi: 10.1155/2012/584257.

Pavan V, Tibaldi S, Brankoviić Č. 2000. Seasonal prediction of blocking frequency: Results from winter ensemble experiments. *Q. J. R. Meteorol. Soc.* **126**: 2125–2142.

Rex DF. 1950a.. Blocking action in the middle troposphere and its effect on regional climate I: The climatology of blocking action. *Tellus* **2**: 196–211.

Rex DF. 1950b.. Blocking action in the middle troposphere and its effect on regional climate II: The climatology of blocking action. *Tellus* **3**: 275–301.

Shadden SC, Lekien F, Marsden JE. 2005. Definition and properties of Lagrangian coherent structures from finite-time Lyapunov exponents in two-dimensional aperiodic flows. *Phys. D* **212**: 271–304.

Shutts GJ. 1983. The propagation of eddies in diffluent jet streams: Eddy vorticity forcing of blocking flow fields. *Q. J. R. Meteorol. Soc.* **109**: 737–761.

Tibaldi S, Molteni F. 1990. On the operational predictability of blocking. *Tellus* **42A**: 343–365.

Watson JS, Colucci SJ. 2002. Evaluation of ensemble predictions of blocking in the NCEP global spectral model. *Mon. Weather Rev.* **130**: 3008–3021.

Wiedenmann JM, Lupo AR, Mokhov II, Tikhonova E. 2002. The climatology of blocking anticyclones for the Northern and Southern Hemisphere: Block intensity as a diagnostic. *J. Clim.* **15**: 3459–3473.

